Regions of very low H3K27me3 partition the *Drosophila* genome into topological domains

Sherif El-Sharnouby[1]*, Bettina Fischer[2,3]*, Jose Paolo Magbanua[1]*, Benjamin Umans[1], Rosalyn Flower[1], Siew Woh Choo[4], Steven Russell[2,3], Robert White[1]

* contributed equally

[1]Department of Physiology, Development and Neuroscience, University of Cambridge, CB2 3DY United Kingdom, [2]Department of Genetics, University of Cambridge, CB2 3EH United Kingdom, [3]Cambridge Systems Biology Centre, University of Cambridge, Tennis Court Road, Cambridge, CB2 1QR United Kingdom, [4]Department of Oral and Craniofacial Sciences, Faculty of Dentistry, University of Malaya, 50603 Kuala Lumpur, Malaysia

Sherif El-Sharnouby	se266@cam.ac.uk
Bettina Fischer	bef22@cam.ac.uk
Jose Paolo Magbanua	jpvm@mac.com
Benjamin Umans	umans@fas.harvard.edu
Rosalyn Flower	rosalyn.flower@crick.ac.uk
Siew Woh Choo	csw1978@hotmail.com
Steven Russell	sr120@cam.ac.uk
Robert White	rw108@cam.ac.uk (corresponding author)

Keywords: chromatin, insulator, architectural protein, histone modification, topologically associated domains, housekeeping genes

Abstract

Background

It is now well established that eukaryote genomes have a common architectural organization into topologically associated domains (TADs) and evidence is accumulating that this organization plays an important role in gene regulation. However, the mechanisms that partition the genome into TADs and the nature of domain boundaries are still poorly understood.

Results

We have investigated boundary regions in the *Drosophila* genome and find that they can be identified as domains of very low H3K27me3. The genome-wide H3K27me3 profile partitions into two states; very low H3K27me3 identifies Depleted (D) domains that contain housekeeping genes and their regulators such as the histone acetyltransferase-containing NSL complex, whereas domains containing mid-to-high levels of H3K27me3 (Enriched or E domains) are associated with regulated genes, irrespective of whether they are active or inactive. The D domains correlate with the boundaries of TADs and are enriched in a subset of architectural proteins, particularly Chromator, BEAF-32, and Z4/Putzig. However, rather than being clustered at the borders of these domains, these proteins bind throughout the H3K27me3-depleted regions and are much more strongly associated with the transcription start sites of housekeeping genes than with the H3K27me3 domain boundaries.

Conclusions

We suggest that the D domain chromatin state, characterised by very low H3K27me3 and established by housekeeping gene regulators, acts to

52 separate topological domains thereby setting up the domain architecture of
53 the genome.
54
55
56
57
58
59
60
61
62
63
64
65
66
67
68
69
70
71
72
73
74
75
76

Background

Our understanding of genome architecture has advanced rapidly in recent years with major insights coming from three approaches; the characterisation of chromatin domains on the basis of their constituent histone marks and associated proteins [1–4], the use of proximity-dependent ligation (3C and derivatives) to define the topology of chromatin within the nucleus [5–9] and the genome-wide mapping of the binding sites of architectural proteins such as the Insulator component, CTCF [10–13]. The combination of these approaches provides a view of the domain organization of the genome with the partitioning of chromatin into topologically associated domains (TADs) linked to the epigenetic landscape of domains of chromatin state and organized by the activities of architectural proteins.

Although the organization of the genome into domains is well established, the processes that form domains and, in particular, the nature of domain boundaries remain unclear. Architectural proteins are enriched at chromatin state domain boundaries; for example CTCF is enriched at the boundaries of H3K27me3 domains [10,12–14]. Architectural proteins are also enriched at TAD boundaries. In vertebrates, the boundaries of megabase-scale TADs show enriched CTCF binding [5]. Subsequent higher resolution studies revealed a refined TAD map with a median TAD size of 185 kb and an association between orientated CTCF binding sites and TAD boundaries, indicating a link between CTCF-dependent chromatin loops and TAD domains [8,15]. In *Drosophila*, TAD boundaries are associated with a number of

architectural proteins, including several Insulator proteins such as CTCF, BEAF-32, CP190 and Insulator-related proteins such as Chromator (also known as Chriz) [9,11]. TAD boundaries are characterised by clusters of architectural protein occupancy and boundary strength correlates with the concentration of architectural protein binding [16]. In several systems, mutations affecting the binding sites of architectural proteins have been shown to lead to reorganization of the domain structure with consequences for gene regulation [17–19]. However, architectural protein binding is not the only genomic feature associated with TAD boundaries; other enriched features include gene density, chromatin accessibility, transcriptional activity and housekeeping genes [5,9,11]. This raises the question of whether the boundaries are simply interfaces between adjacent TADs or whether they are more complex “boundary regions” with inherent activities and whose chromatin structure may act to separate flanking TADs. An interesting property of TAD organization in the genome is that it appears to be highly consistent between different cell types [5,8]. Recent studies suggest that the localization of constitutively expressed housekeeping genes in the regions between TADs may provide a basis for a constant pattern of TADs if the constitutively transcribed inter-TAD regions act to demarcate TAD borders [20,21]. This suggestion also raises questions about the roles of “architectural proteins” such as CTCF, which is implicated in a wide variety of functions. Some appear to be architectural functions, such as its role as a component of Insulator complexes that block enhancer-promoter interaction providing a basis for the establishment of independent regulatory domains in the genome. On the other hand, a significant proportion of CTCF sites occur close to

promoters [22] and CTCF has been shown to promote enhancer-promoter interactions [23–25]. Similarly, the *Drosophila* insulator component BEAF-32 predominantly binds close to transcription start sites (TSSs) and regulates gene expression [26], and the insulator component CP190 is strongly associated with actively transcribed genes [14]. Overall it is unclear whether the clusters of architectural proteins at TAD boundaries provide a straightforward architectural function, acting as barriers demarcating the borders of adjacent TADs, or whether these proteins may be more associated with transcriptional regulation of the genes within the boundary regions.

In this paper we present an investigation into boundary regions in the *Drosophila* genome. We find that they can be identified as domains of very low H3K27me3 levels. The genome-wide H3K27me3 profile partitions into two states; very low H3K27me3 identifies domains that are highly enriched in housekeeping genes whereas domains containing regulated genes, irrespective of whether they are active or inactive, contain mid-to-high levels of H3K27me3. The domains depleted in H3K27me3 correlate with the boundaries of TADs and are enriched in architectural proteins, particularly Chromator, BEAF-32 and Z4/Putzig. However, rather than being clustered at the borders of these domains, these proteins bind throughout the H3K27me3-depleted regions and are much more strongly associated with the TSSs of housekeeping genes than with H3K27me3 domain boundaries. We suggest that the primary function of these proteins is linked to the transcriptional regulation of housekeeping genes and that this activity sets up chromatin

regions that act to separate topological domains, thereby establishing the domain architecture of the genome.

Results

H3K27me3 domains in development

As part of an investigation into changes in the epigenetic landscape during *Drosophila* spermatogenesis, we characterised the profile of the repressive histone mark, H3K27me3, in chromatin from purified primary spermatocytes. The profile is strikingly different to profiles of H3K27me3 found with embryo chromatin. In the embryo data the prominent feature is the enrichment of H3K27me3 in domains containing target sites of Polycomb (Pc) silencing complexes whereas in primary spermatocyte chromatin H3K27me3 appears much more widespread (Fig. 1). Although Pc target domains still show the highest level of H3K27me3 in primary spermatocyte chromatin, much of the genome shows a moderate level of H3K27me3 and domains with a moderate level are clearly distinct from domains where H3K27me3 is very low or absent. Examining other H3K27me3 profiles provides support for a widespread H3K27me3 distribution, for example chromatin from the Kc167 cell line shows significant H3K27me3 in regions matching the moderate domains in primary spermatocytes and also has corresponding regions of very low H3K27me3 (Fig. 1).

To associate levels of H3K27me3 with states of gene expression in primary spermatocytes, we examined the H3K27me3 levels at the TSSs of different gene classes. We find that the lowest levels of H3K27me3 are tightly associated with constitutively expressed (housekeeping) genes (Fig. 1b). In contrast, regulated genes, whether active or inactive, are associated with higher levels of H3K27me3. Induced genes active in primary spermatocytes (spermatogenesis genes) have moderate levels of H3K27me3, whereas inactive genes (not expressed in testis) and Pc targets are associated with higher H3K27me3 levels. In other cells it is also clear that significant levels of H3K27me3 are not only associated with canonical Pc target genes (Fig. 1b,c). A developmental time course indicates that whereas housekeeping genes are always associated with very little or no H3K27me3, the “moderate” class represented by regulated genes (spermatogenesis and not expressed in testis classes) shows increasing H3K27me3 levels. Whilst significantly higher than the housekeeping levels in all profiles, the “moderate” levels are relatively low early in development but then rise to become closer to the level associated with Pc-targets by the pupal stage (Fig. 1d). This suggests that, apart from the housekeeping genes, there is a general developmental increase in H3K27me3 levels outside Pc domains, emphasizing the difference between constitutively active housekeeping regions and the rest of the genome.

H3K27me3 domains provide a binary partitioning of the genome

Focusing on the domains with very little or no H3K27me3 we investigated their associated genomic features (Fig. 2). H3K27me2 exhibits a similar

profile to H3K27me3 with a widespread distribution that has been associated with a global repressive role [27], and we also observe domains of low signal corresponding to the low level domains of H3K27me3. H3K27me3 and H3K27me2 differ at canonical Pc-targets which show high levels of H3K27me3 but low levels of H3K27me2 [27]. The H3K27me3 low level domains also show a link to histone acetylation with a striking match to regions of Histone deacetylase 3 (HDAC3) binding and also a correspondence with regions enriched for MRG15 (a component of the Tip60 Histone acetyl-transferase (HAT) complex, [28,29]), MBD-R2 (a component of the NSL complex which regulates housekeeping gene expression and is associated with the HAT Males absent on the first (MOF) [30–33] and also the H4K16ac modification, generated by MOF and regulated by HDAC3 [34,35].

Applying a Hidden Markov Model to the primary spermatocyte H3K27me3 profile we partitioned the genome into two states, Depleted (D) and Enriched (E) domains (Fig. 2) to facilitate a quantitative analysis of genomic features associated with these regions. There are 1,795 D regions and 1,796 E regions encompassing 34% and 65% of the euchromatic genome respectively. The D regions contain 62% of TSSs and are strongly enriched in housekeeping genes: containing 95% of TSSs of genes in our housekeeping gene class. In contrast, regulated gene classes are associated with E domains. For example, genes whose expression is limited to only a few *Drosophila* cell lines are predominantly in E domains (Fig. 2d). In addition, 75% of embryo Pc targets and 80% of genes specifically activated in spermatocytes are in E domains. Using the five chromatin state classification from Filion et al. [1], we

find that D regions are also enriched in active chromatin states, particularly YELLOW which has previously been associated with housekeeping genes and the Non-Specific Lethal (NSL) complex [32]. While the D regions are depleted in the H3K27me3 and H3K27me2 repressive histone marks, they are enriched for a variety of active marks including H3K4me3, H3K9ac, H3K27ac, H3K36me3 and H4K16ac. Binding of the HAT associated proteins MBD-R2 and MRG15 is enriched in D regions along with HDAC1 and HDAC3. Overall, the distinctive features of D and E domains support the potential functional relevance of this binary partitioning of the genome.

D and E domains and genome architecture

To explore the relationship between the organization of D and E domains and the overall domain architecture of the genome, we generated a high resolution interaction map of the Kc167 cell genome using HiC [6,36] with fragmentation using the 4-base cutter DpnII. As in previous studies, the interaction map shows the organization of the genome into a series of TADs allowing the derivation of a set of TAD boundaries across the genome. The TAD boundaries show a striking coincidence with D/E domain boundaries with 78% of TAD boundaries occurring within one 10kb bin of a D/E boundary (Fig. 3). A similar correspondence is also found with the TAD boundaries defined in embryo chromatin [9]. Comparing the interaction map with the organization of the genome into D and E domains reveals a clear connection, with the prominent interaction-dense TADs generally corresponding to E domains and intervening regions corresponding to D domains (Fig. 3a, Fig. S1). This correspondence has implications for the interpretation of the overall TAD

250 architecture as it suggests that prominent TADs do not simply abut each other
251 with a discrete boundary at the junction. Rather, it suggests a model where
252 neighbouring prominent TADs are separated from each other by an
253 intervening region corresponding to a D domain (Fig. 3c).
254
255 **D domains are rich in a subset of insulator components**
256 The boundaries between TADs are enriched in insulator protein binding; this
257 is seen for CTCF in vertebrates [5,8,15] and for a number of insulator
258 components in *Drosophila* [9,11,13,16]. We analysed insulator component
259 binding in D domains, using published profiles (Fig. 4). We find a strong
260 association between the binding of the insulator protein BEAF-32 and D
261 domains, with 86% of BEAF-32 binding sites mapping to D domains. BEAF-32
262 binding is known to be largely overlapping with the insulator-related protein
263 Chromator [37], the factor most strongly associated with TAD boundaries in
264 embryo chromatin [9] and which directly interacts with BEAF-32 to form a
265 complex that recruits CP190 [37]. We find Chromator is also strongly enriched
266 in D domains, with 88% of sites mapping to D regions. Chromator forms a
267 complex with Z4/Putzig that recruits the JIL-1 kinase to promote H3S10
268 phosphorylation [38,39] and we find Z4/Putzig binding almost entirely confined
269 to D domains with 96% of sites mapping to D regions. Whilst BEAF-32,
270 Chromator and Z4/Putzig form a strongly D-associated group, the insulator
271 component CP190, which is recruited to chromatin by several distinct DNA-
272 binding insulator proteins including BEAF-32, CTCF and Su(Hw), is more
273 widely distributed with only 66% of binding sites in D regions. As over 70% of
274 CP190 sites within D regions overlap with BEAF-32 binding, this suggests that

the CP190 in D domains is specifically recruited into BEAF-32 insulator complexes. The insulator components GAF and CTCF are also widely distributed and lack a strong association with D domains. The Su(Hw) insulator protein has a distinct distribution, being relatively depleted from D domains, with only 26% of sites in D regions.

Although insulators have previously been associated with the borders of chromatin state domains, it is striking that the D domain-associated components BEAF-32, Chromator and Z4/Putzig are distributed quite evenly across D regions rather than being concentrated at the D/E boundaries (Fig. 4c and d). This argues against the idea that insulator complexes are simply positioned at the boundaries of chromatin state domains.

As several *Drosophila* insulator proteins have previously been shown to be enriched at promoters, we examined the association between architectural protein binding and housekeeping gene TSSs. BEAF-32, Chromator, CP190 and Z4/Putzig all show strong enrichment at housekeeping TSSs. Comparing the enrichments at housekeeping TSSs versus D/E borders we find much more enrichment at TSSs than borders. CTCF shows less strong enrichment at housekeeping TSSs, but interestingly it is still more strongly enriched at housekeeping TSSs than at D/E domain borders (Fig. 4e).

D and E domains are topologically distinct

As noted above, the E regions generally correspond to prominent TADs, i.e. regions of enhanced interaction with widespread interactions across the

domains (Fig. 3). In contrast, D domains, even if they are long, have a different appearance in the interaction map with less prominent long-range interactions (Fig. 5). This difference is evident in a plot of short-range (5-50kb) versus long-range (50–500kb) interactions where the D domains correspond to regions with high short-range versus long-range interaction ratios. Accumulating the interaction length data across the genome, we find that D and E domains have significantly different profiles (Fig. 5b) with D domains associated predominantly with short-range interactions and a more rapid fall in interaction density with increasing interaction length.

Interaction of D domains

In the genomic interaction maps there is evidence for interaction between D regions. This is seen as areas of enhanced interaction that sit on top of E TADs, corresponding to interaction between the two D domains that flank the E TAD (Figs. 1 and 6). Although they are not present at all E domains, such D-D interaction regions are frequently observed. For example, if we take the 174 E domains of 60kb or above that are flanked on both sides by D domains, we find that 61 (35%) are associated with D-D interaction regions that contain more than 1.1-fold higher interaction density in the D-D region compared to neighbouring bins. A further feature of the interaction map, exemplified in Fig. 6, is that E domain TADs are frequently flanked by a zone of relatively reduced interaction, corresponding to the zone of D-E interactions. The relative lack of interaction in this zone compared to neighbouring E-E and D-D interaction zones suggests that, whilst nearby homologous regions interact,

there is less heterologous (D-E) interaction suggesting spatial segregation of D and E regions in the nucleus.

Discussion

In this paper we propose a fundamental binary partitioning of the genome based on chromatin state. We identify two domain states based on the level of H3K27me3: Depleted or D domains having little or no H3K27me3 and Enriched or E domains with significant levels of H3K27me3. These two domain states differ markedly in their genomic features. In particular, the D domains are enriched in housekeeping gene TSSs, in regulators of housekeeping genes such as the histone acetyltransferase-containing NSL complex and in a subset of insulator and insulator-related components including BEAF-32, Chromator and Z4/Putzig. In contrast, the E domains are enriched in tissue-specific genes suggesting that the D/E divide may represent a binary subdivision between the constitutive and regulated genome. The organization of D and E domains is strongly associated with the topological architecture of the genome, supporting the idea that the constant TAD organization identified in several studies may be based on prominent TADs being flanked by domains enriched in constitutive gene expression. The prominent TADs correspond to E domains and are flanked by D domains rich in housekeeping genes. This proposed binary subdivision on the basis of D and E domains is likely to be related to the long-observed binary subdivision of the *Drosophila* genome based on the banding pattern of polytene chromosomes with D domains, rich in inter-band-specific proteins such as

Chromator, Z4/Putzig and MRG15, representing inter-bands and E domains representing chromosomal bands.

Although we propose a constant partitioning of the genome based on the H3K27me3 profile, the level of H3K27me3 in the E domains is dynamic. Early in development H3K27me3 is focused on Pc target genes, whereas later in development H3K27me3 is at moderate/high levels throughout E domains and this is particularly apparent in the profile from purified germline cells from the adult testis. Increased spreading of the H3K27me3 mark during development has been noted in mammalian genomes [40]. There is also a clear relationship between the widespread H3K27me3 we observe later in development and the profile of H3K27me2, which shows pervasive binding in E domains (except for Pc target regions) [27]. Inhibition of PRC2 histone methylase leads to loss of both H3K27me2 and me3 and is accompanied by a widespread increase in transcriptional activity not just at Pc target genes [27]. Pervasive H3K27me2 is proposed to be governed by opposing roaming activities of PRC2 and the UTX demethylase complexes. This mechanism, together with an active role in widespread gene repression, may also apply to the H3K27me3 in E domains.

The striking correspondence of the D domains, defined by chromatin state, with the regions flanking prominent TADs suggests that the genomic distribution of chromatin state domains may have a key role in establishing the genome interaction architecture. What are the features of D domains that could enable them to function as boundary regions or inter-TADs? Although

very low levels of H3K27me3 define D domains, this histone mark seems unlikely to be the key functional property since it is dynamic, in contrast to the TAD organization, which appears to be constant. The chromatin state characteristics of D domains include little or no H3K27me2 and enrichment for active marks such as H3K36me3 and H4K16ac. The major enzyme responsible for acetylation of H4K16 is MOF [35], a component of the NSL complex that regulates housekeeping genes [31,32] and D domains are enriched in the NSL component MBD-R2. H4K16ac is a candidate for a modification with an effect on genome architecture as it has been demonstrated to affect chromatin structure [41]. It is interesting that HAT complexes and HDACs (particularly HDAC3 which targets H4K16ac [34]) are both enriched in D domains, however both are associated with gene expression in a mechanism whereby the H3K36me3 mark, linked with elongating PolII, recruits HDACs to inhibit inappropriate initiation within active transcription units [42–44]. A further modification that may be relevant to an architectural role of D domains is H3S10 phosphorylation mediated by JIL-1 kinase, which is recruited to polytene chromosome interband regions by a complex containing Chromator and Z4/Putzig [39]. Mutations in JIL-1 kinase, Chromator and Z4/Putzig all result in disruption to polytene chromosome structure [38,39,45–47]. Overall, we envisage that housekeeping transcription factors and a subset of insulator components recruit chromatin modification complexes leading to the establishment of the D chromatin state. The observed TAD organization could be dependent on the different properties of the D and E chromatin states. As suggested and modelled by Ulianov et al. [21], TAD organization can be generated based on two domain states with

399 differing chromatin aggregation properties. We have shown that D and E
400 domains differ in their interaction properties (Fig. 5) with E domains showing a
401 rather even high density of interactions across the domain, consistent with
402 condensed chromatin, and D domains being characterised by shorter range
403 interactions. Differential interaction properties are also supported by the
404 observation of decreased interaction between neighbouring D and E regions
405 and increased interaction between nearby D domains (Fig. 6), suggesting
406 spatial segregation of the two domain states.
407
408 Insulator proteins have been proposed to be key mediators of both genome
409 architecture and chromatin state domains. Our analysis has implications for
410 insulator complex function since we do not find insulator protein binding to be
411 strongly associated with the D/E chromatin state boundaries. The binding of a
412 subset of insulator components is enriched in D domains but these
413 components bind throughout the D domains and are strongly associated with
414 the TSSs of housekeeping genes, not with domain boundaries. This suggests
415 that insulator components, at least in the BEAF-32/Chromator/CP190 context,
416 may be more directly associated with transcriptional regulation than with
417 chromatin state boundary formation. BEAF-32 has been linked to transcription
418 and in *BEAF-32* mutants many BEAF-32-associated genes show reduced
419 expression [26]. In addition, Chromator acts as a transcriptional activator with
420 specificity for housekeeping promoters [48]. We suggest that at least part of
421 the contribution of BEAF-32, Chromator and CP190 to genome architecture
422 may be indirect as they may act to establish the chromatin state in D domains,
423 for example by recruiting chromatin modifiers such as JIL-1 kinase, enabling

D domains to act as boundary regions flanking TADs. As BEAF-32/Chromator/CP190 complexes mediate DNA interactions [37] and D domains are characterised by short-range looping, the insulator complexes may be mediating loop formation within D domains potentially forming promoter/promoter or promoter/enhancer contacts. The idea that insulator complexes within D domains are primarily involved with transcriptional regulation leaves open the question of what actually determines the location of the D/E boundaries. We speculate that the location of the chromatin state boundaries may be specified, not by insulator complexes precisely at the boundary, but by the range of action of chromatin modification complexes that are recruited to D domains by the insulator complexes and other transcription factors.

Despite a considerable body of evidence from studies on the mammalian genome linking the insulator protein CTCF with the domain organization of the genome, we find little association between CTCF binding and the D/E domain organization defined by H3K27me3 levels. Here our studies agree with Ulianov et al. [21], where HiC experiments on several *Drosophila* cell lines found that CTCF was only weakly enriched at regions separating TADs, and with Sexton et al. [9] who found in a genome-wide 3C analysis of embryo chromatin that Chromator is considerably more strongly associated with topological boundaries than CTCF. On the other hand, CTCF is clearly associated with domain architecture as it flanks Pc-regulated domains in Hox complexes [19,49,50] and mutating CTCF sites disrupts these domains [19]. Sexton et al. [9] find that CTCF is preferentially associated with borders of Pc

449 domains. This suggests that, at least in *Drosophila*, CTCF may mediate the
450 formation of a specialized set of domains distinct from the more general D/E
451 domain organization of the genome.
452
453 **Conclusion**
454 We propose a binary partitioning of the genome based on chromatin state that
455 provides a basis for the organization of chromatin into TADs and that reveals
456 an architectural distinction between the organization of constitutive and
457 regulated genes.
458
459 **Methods**
460 **ChIP-array on Primary Spermatocytes**
461 *Fly stocks*: For sorting YFP^{+} primary spermatocytes, we used homozygous
462 males of the YFP-tagged protein-trap line *heph*^{CPTI002406} [51] which is
463 homozygous fertile.
464 *Testis dissections, cell extraction and fixation*: Testes were dissected in ice-
465 cold Schneider's medium (supplemented with 10% fetal calf serum) and
466 incubated with collagenase (5 mg ml^{-1}, Sigma-Aldrich C8051) plus protease
467 inhibitors (Sigma-Aldrich P8340) in medium for 5 min at room temperature.
468 After washing in medium, cells were extracted by gently pipetting for 5 min in
469 100 µl medium, using a P200 tip (Rainin RT-200F; with 1.5 mm of the tip cut
470 off to increase the diameter of the opening) and fixed by adding an equal
471 volume of 2% formaldehyde (Sigma-Aldrich F8775) in PBS. Cells were mixed
472 thoroughly and incubated for 10 min at 23°C in an Eppendorf Thermomixer at
473 700 rpm. Fixation was stopped by adding 400 µl ice-cold medium and placing

the sample on ice. The sample was centrifuged in a swing-out rotor at 1,000 *g* for 5 min at 4°C and the pellet snap frozen in liquid N_2 prior to storage at −80°C. A total of 1,000 testes were dissected for each ChIP-array replicate. Testes were dissected in batches of 100 and, for each batch, the time from the start of dissection until fixation was approximately 1 hr.

FACS: Aliquots of extracted cells stored at −80°C were thawed, combined in PBS/0.01% Triton X-100 and passed through a 50 µm filter (Partec 04-004-2327). Cells were sorted using a 100 µm nozzle on a MoFlo FACS machine (Beckman Coulter) equipped with a 488 nm argon laser (100 mW). Cells were sorted into a microfuge tube containing 700 µl PBS/0.01% Triton X-100. Events were triggered on forward scatter and YFP^+ events were sorted using the gating strategy described in Fig. S2. Data was acquired and analysed using Summit software (Beckman Coulter).

ChIP on sorted cells: Sorted cells were centrifuged in a swing-out rotor at 4,000 *g* for 15 min at 4°C, transferred to a thin-walled 0.5 ml microfuge tube (Axygen PCR-05-C), re-centrifuged and then resuspended in 130 µl Lysis Buffer (17 mM Tris.HCl (pH 8), 3.4 mM EDTA.Na_2, 0.34% SDS) containing protease inhibitors (Sigma-Aldrich P8340). The lysate was sonicated for 5 cycles at high setting using a Diagenode Bioruptor (1 cycle is 30 s ON and 30 s OFF). After sonication, the sample was centrifuged at 16,000 *g* for 15 min at 4°C, the chromatin-containing supernatant transferred to a fresh microfuge tube and 70 µl RIPA buffer (36.7 mM Tris.HCl (pH 8), 2.5 mM EDTA.Na_2, 0.01% SDS, 2.46% Triton X-100, 374 mM NaCl) containing protease inhibitors added to the chromatin sample. The ChIP reaction, washes and DNA purification were performed as in Dahl and Collas [52,53]. In brief,

magnetic beads were coated with 2.4 µg of rabbit anti-H3K27me3 antibody (Millipore 07-449) and incubated overnight in a volume of 100 µl with chromatin from ~100,000 YFP^+ sorted cells. Beads were washed, chromatin eluted, RNA and proteins digested, the DNA purified by phenol/chloroform extraction followed by ethanol precipitation using linear acrylamide as carrier and resuspended in 10 µl PCR grade water. Approximately 5 µl of chromatin was retained as input and purified alongside the ChIP sample.

Amplification and labelling of ChIP DNA: ChIP and input DNA were amplified using the GenomePlex Single Cell Whole Genome Amplification Kit (Sigma-Aldrich WGA4) following the manufacturer's instructions from the library preparation stage. Approximately 150 pg of DNA was used for amplification. Samples were amplified for 22 cycles and amplified DNA was purified using a QIAquick PCR Purification Kit (Qiagen). The amplified ChIP and input DNA (2 µg each) were labelled with Cy5 and Cy3 using the BioPrime DNA Labeling Kit (Invitrogen) in the presence of Cy3- or Cy5-dCTP (GE Healthcare) and hybridised onto Nimblegen ChIP-chip 2.1M Whole-Genome Tiling Arrays according to the manufacturer's instructions.

Microarray data processing: We performed two biological replicates with a Cy3/Cy5 dye swap. Input chromatin was used as the reference to determine ChIP enrichment. Arrays were scanned and the images processed using NimbleScan software to generate raw data (*.pair) files for each channel. Loess spatial correction was performed using the NimbleScan software and an in-house R script was used to generate normalised $\log_2$ ChIP/input ratio (*.sgr) files. For each array the median intensity per channel was scaled to 500 then quantile normalisation was performed across all channels. The

524 normalised ratio scores for both arrays were averaged then smoothed by
525 computing the mean score per 1 kb tiling window. The resulting *.bedgraph
526 file was visually examined using the Integrated Genome Browser [54].

527 **HiC**

528 HiC protocol was based on the methods described in [6,36,55].

529 *Cell Collection*: Kc167 cells (obtained from the *Drosophila* Genomics
530 Resource Center) were cultured in 10cm Petri plates in Schneider's medium
531 supplemented with 5% fetal calf serum and antibiotics at 25°C. Cells from 6
532 plates were harvested into sterile 50 ml centrifuge tubes. The cells were
533 collected by centrifugation at 1,200 rpm for 5 min at 4°C then re-suspended in
534 10 ml fresh medium and the cell concentration determined using a
535 haemocytometer. 1 x10^8 cells were resuspended to a total volume of 45 ml in
536 fresh medium, fixed by the addition of 1.25 ml 37% formaldehyde solution and
537 incubated with gentle shaking on a platform shaker at room temperature for
538 10 min. The reaction was stopped by adding 2.5 ml 2.5M glycine and further
539 incubation at room temperature for 5 min followed by 15 min on ice. The
540 cross-linked cells were divided into 4 x 15 ml falcon tubes (~12.3 ml per tube)
541 and collected by centrifugation at 1,500 rpm for 10 min at 4°C. The
542 supernatant was discarded and the fixed cells were flash frozen in liquid N_2
543 then stored at -80°C.

544 *Restriction enzyme digestion*: Cells were thawed on ice (~2.0 x10^7 cells) and
545 500 µl of lysis buffer (10 mM Tris-Cl, pH 8.0; 10 mM NaCl, 0.2% Igepal
546 CA360) and 50 µl of protease inhibitor cocktail (Sigma) were added. Cells
547 were lysed with 15 strokes of a Dounce homogeniser using the tight pestle
548 (Pestle A). The cell suspension was transferred to a microcentrifuge tube and

549 centrifuged at 5,000 rpm at room temperature for 5 min. The supernatant was
550 discarded, the pellet washed twice with 0.5 ml of ice-cold 1.20x NEBuffer 3
551 (5,000 rpm, 5 min at room temperature) and the pellet resuspended in 500 µl
552 of ice-cold 1.20x NEBuffer 3. 7.5 µl of 20% SDS was added and the sample
553 incubated at 37°C with shaking at 900 rpm for 1h, 50 µl of 20% Triton X-100
554 was added and incubation continued at 37°C, 900 rpm for 1h. A 50 µl aliquot
555 was taken and stored at -20 °C to serve as undigested control. 45 µl of 1.20x
556 NEBuffer 3 was then added to the remaining lysate followed by 400 U (8 µl) of
557 50U/µl DpnII and the digestion reaction was incubated at 37°C with shaking at
558 900 rpm overnight.

559 *Blunt ending fragments with Klenow enzyme*: The restriction enzyme reaction
560 was incubated at 65°C for 20 min to inactivate DpnII, then dispensed into five
561 100µl aliquots in fresh microfuge tubes. Tube 1 was designated as a 3C
562 control and Tubes 2-5 were used as Hi-C samples. To the Hi-C samples 0.35
563 µl each of 10 mM dCTP, dGTP and dTTP, 8.75 µl of 0.4 mM biotin-14-dATP
564 and 5 µl of 5U/µl Klenow enzyme (NEB M210S) were added followed by
565 incubation at 37°C for 45 min.

566 *Ligation*: 200 µl of 10 mM Tris-HCl/1% SDS was added to each blunt-ended
567 reaction and the 3C control tube, followed by transfer to a fresh 50 ml tube
568 containing 700 µl 10x T4 DNA Ligase Buffer (NEB) and 5894 µl molecular
569 biology grade water. Then 106 µl 20% Triton X-100 was added and the
570 mixture incubated for 1 h at 37°C with gentle shaking. 10,000U of DNA ligase
571 (NEB, M0202L) was added and then incubated for 18h at 16˚C followed by 30
572 min at room temperature.

573 *De-crosslinking and DNA purification*: 30 µl of 10 mg/ml Proteinase K (300 µg
574 final) was added to the reaction and incubated at 65˚C overnight. 10 µl of 30
575 mg/ml RNase A (Sigma) was added and the reaction was incubated at 37˚C
576 for 45 min. 7 ml phenol-chloroform-isoamyl alcohol (PCI) was added and
577 mixed vigorously by vortexing. The mixture was transferred to a 50 ml Phase
578 Lock Gel tube (5 Prime, 2302860) and centrifuged at 2,200 g for 15 min at
579 room temperature. The aqueous phase was transferred to a fresh 50 ml tube
580 and 7 ml of distilled water, 1.5 ml 3M NaAcetate pH 5.2, and 35 ml 100% ice-
581 cold ethanol were added. The mixture was incubated at -80°C for 1 h then
582 centrifuged at 2,200 g, 4°C, for 45 minutes. The pellet was washed with 10 ml
583 70% ethanol, centrifuged at 2,200 g at 4°C for 15 min and the pellet dried at
584 room temperature for 10-15 min. The pellet was then re-suspended in 150 µl
585 of 10 mM Tris-HCl pH 8.0 and allowed to dissolve overnight at 4°C. The
586 purified DNA was then transferred to a microcentrifuge tube and stored at -
587 20°C.

588 *Re-purification of DNA*: 150 µl of 10 mM Tris-HCl pH 8.0 was added to the
589 dissolved pellet followed by 300 µl Phenol-ChIoroform. These were then
590 mixed and centrifuged at 13,200 rpm for 5 min at room temperature in a
591 Phase Lock tube. Phenol-ChIoroform extraction was then repeated on the
592 aqueous phase and DNA was precipitated by adding 30 µl 3M NaAcetate, pH
593 5.2 and 2.5 volumes of ice-cold 100% ethanol. The mixture was incubated at -
594 80˚C for at least 45 min then centrifuged for 20 min at 13,200 rpm at 4˚C. The
595 pellet was washed with 0.5 ml of ice-cold 70% ethanol and air-dried briefly.
596 The pellet was then resuspended in 25 µl TLE Buffer **(**10 mM Tris-Cl pH 8.0,
597 0.1 mM EDTA). The Hi-C DNA preparations were pooled into a single tube

and the concentration measured using a Qubit photometer.

Removal of biotin from unligated ends and shearing of Hi-C DNA: For every 5 µg of Hi-C DNA preparation, the following were added: 1 µl 10 mg/ml BSA, 10 µl 10X NEBuffer 2, 1 µl 10mM dGTP, 1.67 µl (5U) T4 DNA polymerase and water to a total volume of 100 µl. The mixture was incubated at 12°C for 2 hr and the reaction stopped by adding 2 µl 0.5 M EDTA pH 8.0. DNA was then purified by adding 1 volume of Phenol-ChIoroform and centrifuging at 13,200 rpm for 5 min at room temperature in a Phase Lock tube. The DNA in the aqueous phase was precipitated by adding 10 µl 3M NaAcetate, pH 5.2 and 2.5 volumes ice-cold 100% ethanol. The mixture was incubated at -80°C for at least 30 min then centrifuged for 20 min at 13,200 rpm at 4◦C. The pellet was washed with 0.5 ml of ice-cold 70% ethanol, then dissolved and pooled in a total volume of 100 µl of water. The Hi-C DNA preparation was sheared at 4°C for 20 min in 30 sec pulses at low setting using a Bioruptor sonicator (Diagenode).

Library Preparation: 1.5 µg sheared DNA was end repaired, poly-A tailed and adapters added using the TruSeq Kit (Illumina). The adapter ligated Hi-C library was run on a 1.5% agarose gel in 0.5X TBE at 50V for 2 h. The gel was stained with Sybr Gold and DNA fragments ~250 to 750 bp in size were excised and purified using a Qiagen Gel Extraction Kit. The DNA was eluted with 50 µl of TLE buffer and the final volume adjusted to 300 µl with water. Biotin-tagged size-selected Hi-C DNA was purified using Dynabeads MyOne Streptavidin Beads (Invitrogen). 150 µl of resuspended beads were prepared according to the manufacturer's instructions. These were then re-suspended

in 300 µl 2x Binding Buffer (10 mM Tris-HCl pH 8.0, 1 mM EDTA, 2 M NaCl) and combined with 300 µl of repaired Hi-C DNA. The biotin-labelled Hi-C DNA was incubated with the streptavidin beads at room temperature for 15 min on a rotator. The beads were then washed in 400 µl 1x Binding Buffer followed by a single wash with 100µl 1x ligase buffer. The beads were then re-suspended in 50µl 1x ligase buffer and submitted to the Eastern Sequence and Informatics Hub (EASIH, Cambridge) for library preparation and 76-bp paired-end sequencing on an Illumina GAIIx sequencer.

HiC data and segments

Paired-end HiC reads were aligned against *Drosophila* genome BDGB release 5 with HiCUP (v0.5.7) [56]. Read counts/filtering are given in Table S1. Interactions were binned at 10 kb resolution. Contact matrices were normalised using the GOTHiC_1.6.0 R package [57]. HiC segments were identified from the normalised contact matrices using the HiCseg R package [58], with 10% of the lowest linear portion of log-likelihood segment borders removed.

Gene Classes and H3K27me3 developmental profile

Housekeeping genes (4,091 genes) were derived from FlyAtlas [59] selecting genes expressed in all tissues (4 present calls), spermatogenesis genes (1,428 genes) were from Chen et al. [60] (GEO accession GSE28728) selecting genes down-regulated 4-fold or more in *aly* mutant testes, not-expressed-in-testis (2,432 genes) were from FlyAtlas selecting genes with zero calls in testis and >4 positive calls across other tissues and

Polycomb_target genes (359 genes) were from Kwong et al. [61]. Genome annotation was Flybase Release 5.57 and the "all" class includes all genes in the euchromatic genome (13,832 TSSs). Raw ChIP-chip files of H3K27me3 in *Drosophila* at different time points of development were downloaded from GEO GSE15423. The data was quantile normalised for each time point and average scores across replicates calculated. Median scores for all gene TSSs (+/- 500bp) were calculated for each developmental stage. For the relative distance analysis, the mean scores of housekeeping, Pc and spermatogenesis TSSs were calculated for each stage. The distance between housekeeping and Pc class means was set to 1 and the relative distance of the spermatogenesis class mean to the housekeeper mean was calculated.

H3K27me3 Hidden Markov Model (HMM)

Normalised Spermatocyte H3K27me3 euchromatin oligo scores were binned at 1 kb resolution taking the mean score per bin. A HMM using normal distribution was fitted for two states using the RHmm R package [62] for each chomosome. This divided the data into D (depleted in H3K27me3) and E (enriched in H3K27me3) bins. Adjacent bins with the same HMM state were then combined into regions. Gaps in the genome for which there were no oligo probes were closed if the same state was present on both sides.

Binding data

ChIP-chip .cel files were downloaded from ModENCODE [63] for Chromator (277), CTCF (908), GAF (2568) and Jil1 (3037) and processed with Ringo [64] using a half window of 300 bp, minProbes 8 and max gap 200 bp. Binding

672 regions were called using a False Discovery Rate (FDR) of 1%. ChIP-seq
673 fastq data was downloaded from GEO for BEAF32 (GSM1535963), CP190
674 (GSM1535980), Z4/Putzig (GSM1536022) [65] and Su(Hw) (GSM762839)
675 [66]. Reads were mapped to *Drosophila* genome BDGB release 5 using
676 Bowtie with -m 1 option. ChIP-seq peaks were called with macs2 2.1.0
677 (https://github.com/taoliu/MACS) [67] using unique tags and a q-value
678 threshold of 1e-6 and otherwise the default parameters. Data sources are
679 given in Table S2.

680 **Fraction of genes in class**

681 Gene expression score data for 25 *Drosophila* cell lines were downloaded
682 from Supplemental Table S-3 of Cherbas et al. [68]. These gene scores
683 derived from whole-genome tiling microarrays and represent the normalised
684 maximum score for all exons included in that gene. Genes were assigned to D
685 and E regions based on the location of the TSS. As suggested by Cherbas et
686 al. we selected a threshold score of 300 to distinguish the expressed from
687 unexpressed genes. For each gene we counted in how many cell lines it had
688 an expression score > 300, and calculated the fractions of expressed genes in
689 D and E.

690

691 **Interaction Fractions**

692 HiC interactions were binned at 5kb resolution and normalised using GOTHiC.
693 Interactions for each 5 kb genomic bin up to 1 Mb distance were collected,
694 excluding genomic coordinates located within 1 Mb of the chromosome ends.
695 The sum of the interactions for each bin were set to 1 and fractions for close
696 (5-50kb, thus ignoring interactions which are within 5kb of each other) and far

(50-500kb) calculated. Bins with no interactions and bins with extreme high interaction sum (> 97.5th percentile) were excluded. The ratio is given as fraction close/fraction far.

Declarations

Ethics approval and consent to participate

n/a

Consent for publication

n/a

Availability of data and material

The datasets generated during and/or analysed during the current study are available at GEO (Accession number GSE85504)

Competing interests

The authors declare that they have no competing interests.

Funding

This work was supported by the Wellcome Trust (grant 089834/Z/09/Z), by the University of Malaya High Impact Research (grant UM.C/625/HIR/MOHE/CHAN-08) from the Ministry of Higher Education Malaysia, and by the BBSRC (grant BB/M007081/1). BU was funded by a Cambridge Marshall Scholarship.

Authors' Contributions

SE, JPM, SWC, SR and RW conceived and supervised experiments. SE and JPM performed the experiments. SE, BF, BU, RF and RW analysed data. SE, BF, JPM, SR and RW wrote the paper. All authors read and approved the final manuscript.

Acknowledgements

n/a

Additional Files

Additional File 1: Fig. S1. The comparison of Kc cell and embryo interaction maps. (PDF 1.2MB)

Additional File 2: Fig. S2. The purification of primary spermatocytes by FACS. (PDF 3.5MB)

Additional File 3: Table S1 HiC/HiCUP read counts and filtering. (XLSX 11KB)

Additional File 4: Table S2 Data sources. (XLSX 11KB)

References

1. Filion GJ, van Bemmel JG, Braunschweig U, Talhout W, Kind J, Ward LD, et al. Systematic protein location mapping reveals five principal chromatin types in Drosophila cells. Cell. 2010;143:212–24.

2. Hoffman MM, Ernst J, Wilder SP, Kundaje A, Harris RS, Libbrecht M, et al. Integrative annotation of chromatin elements from ENCODE data. Nucleic Acids Res. 2012;gks1284.

3. Kharchenko PV, Alekseyenko AA, Schwartz YB, Minoda A, Riddle NC, Ernst J, et al. Comprehensive analysis of the chromatin landscape in Drosophila melanogaster. Nature. 2011;471:480–5.

4. Yip KY, Cheng C, Bhardwaj N, Brown JB, Leng J, Kundaje A, et al. Classification of human genomic regions based on experimentally determined binding sites of more than 100 transcription-related factors. Genome Biol. 2012;13:R48.

5. Dixon JR, Selvaraj S, Yue F, Kim A, Li Y, Shen Y, et al. Topological domains in mammalian genomes identified by analysis of chromatin interactions. Nature. 2012;485:376–80.

6. Lieberman-Aiden E, van Berkum NL, Williams L, Imakaev M, Ragoczy T, Telling A, et al. Comprehensive mapping of long-range interactions reveals folding principles of the human genome. Science. 2009;326:289–93.

7. Nora EP, Lajoie BR, Schulz EG, Giorgetti L, Okamoto I, Servant N, et al. Spatial partitioning of the regulatory landscape of the X-inactivation centre. Nature. 2012;485:381–5.

755 8. Rao SSP, Huntley MH, Durand NC, Stamenova EK, Bochkov ID, Robinson
756 JT, et al. A 3D map of the human genome at kilobase resolution reveals
757 principles of chromatin looping. Cell. 2014;159:1665–80.

758 9. Sexton T, Yaffe E, Kenigsberg E, Bantignies F, Leblanc B, Hoichman M, et
759 al. Three-dimensional folding and functional organization principles of the
760 Drosophila genome. Cell. 2012;148:458–72.

761 10. Cuddapah S, Jothi R, Schones DE, Roh T-Y, Cui K, Zhao K. Global
762 analysis of the insulator binding protein CTCF in chromatin barrier regions
763 reveals demarcation of active and repressive domains. Genome Res.
764 2009;19:24–32.

765 11. Hou C, Li L, Qin ZS, Corces VG. Gene density, transcription, and
766 insulators contribute to the partition of the Drosophila genome into physical
767 domains. Mol. Cell. 2012;48:471–84.

768 12. Nègre N, Brown CD, Shah PK, Kheradpour P, Morrison CA, Henikoff JG,
769 et al. A comprehensive map of insulator elements for the Drosophila genome.
770 PLoS Genet. 2010;6:e1000814.

771 13. Van Bortle K, Ramos E, Takenaka N, Yang J, Wahi JE, Corces VG.
772 Drosophila CTCF tandemly aligns with other insulator proteins at the borders
773 of H3K27me3 domains. Genome Res. 2012;22:2176–87.

774 14. Bartkuhn M, Straub T, Herold M, Herrmann M, Rathke C, Saumweber H,
775 et al. Active promoters and insulators are marked by the centrosomal protein
776 190. Embo J. 2009;28:877–88.

777 15. Gómez-Marín C, Tena JJ, Acemel RD, López-Mayorga M, Naranjo S,
778 Calle-Mustienes E de la, et al. Evolutionary comparison reveals that diverging
779 CTCF sites are signatures of ancestral topological associating domains
780 borders. Proc. Natl. Acad. Sci. 2015;112:7542–7.

781 16. Van Bortle K, Nichols MH, Li L, Ong C-T, Takenaka N, Qin ZS, et al.
782 Insulator function and topological domain border strength scale with
783 architectural protein occupancy. Genome Biol. 2014;15:R82.

784 17. Guo Y, Xu Q, Canzio D, Shou J, Li J, Gorkin DU, et al. CRISPR Inversion
785 of CTCF Sites Alters Genome Topology and Enhancer/Promoter Function.
786 Cell. 2015;162:900–10.

787 18. Lupiáñez DG, Kraft K, Heinrich V, Krawitz P, Brancati F, Klopocki E, et al.
788 Disruptions of topological chromatin domains cause pathogenic rewiring of
789 gene-enhancer interactions. Cell. 2015;161:1012–25.

790 19. Narendra V, Rocha PP, An D, Raviram R, Skok JA, Mazzoni EO, et al.
791 CTCF establishes discrete functional chromatin domains at the Hox clusters
792 during differentiation. Science. 2015;347:1017–21.

793 20. Eagen KP, Hartl TA, Kornberg RD. Stable Chromosome Condensation
794 Revealed by Chromosome Conformation Capture. Cell. 2015;163:934–46.

795 21. Ulianov SV, Khrameeva EE, Gavrilov AA, Flyamer IM, Kos P, Mikhaleva
796 EA, et al. Active chromatin and transcription play a key role in chromosome
797 partitioning into topologically associating domains. Genome Res.
798 2015;gr.196006.115.

799 22. Kim TH, Abdullaev ZK, Smith AD, Ching KA, Loukinov DI, Green RD, et
800 al. Analysis of the vertebrate insulator protein CTCF-binding sites in the
801 human genome. Cell. 2007;128:1231–45.

802 23. Ing-Simmons E, Seitan VC, Faure AJ, Flicek P, Carroll T, Dekker J, et al.
803 Spatial enhancer clustering and regulation of enhancer-proximal genes by
804 cohesin. Genome Res. 2015;25:504–13.

805 24. Majumder P, Scharer CD, Choi NM, Boss JM. B cell differentiation is
806 associated with reprogramming the CCCTC binding factor-dependent
807 chromatin architecture of the murine MHC class II locus. J. Immunol. Baltim.
808 Md 1950. 2014;192:3925–35.

809 25. Patel B, Kang Y, Cui K, Litt M, Riberio MSJ, Deng C, et al. Aberrant TAL1
810 activation is mediated by an interchromosomal interaction in human T-cell
811 acute lymphoblastic leukemia. Leukemia. 2014;28:349–61.

812 26. Jiang N, Emberly E, Cuvier O, Hart CM. Genome-wide mapping of
813 boundary element-associated factor (BEAF) binding sites in Drosophila
814 melanogaster links BEAF to transcription. Mol Cell Biol. 2009;29:3556–68.

815 27. Lee H-G, Kahn TG, Simcox A, Schwartz YB, Pirrotta V. Genome-wide
816 activities of Polycomb complexes control pervasive transcription. Genome
817 Res. 2015;25:1170–81.

818 28. Cai Y, Jin J, Tomomori-Sato C, Sato S, Sorokina I, Parmely TJ, et al.
819 Identification of new subunits of the multiprotein mammalian TRRAP/TIP60-
820 containing histone acetyltransferase complex. J. Biol. Chem.
821 2003;278:42733–6.

822 29. Kusch T, Florens L, Macdonald WH, Swanson SK, Glaser RL, Yates JR,
823 et al. Acetylation by Tip60 is required for selective histone variant exchange at
824 DNA lesions. Science. 2004;306:2084–7.

825 30. Cai Y, Jin J, Swanson SK, Cole MD, Choi SH, Florens L, et al. Subunit
826 composition and substrate specificity of a MOF-containing histone
827 acetyltransferase distinct from the male-specific lethal (MSL) complex. J. Biol.
828 Chem. 2010;285:4268–72.

829 31. Feller C, Prestel M, Hartmann H, Straub T, Söding J, Becker PB. The
830 MOF-containing NSL complex associates globally with housekeeping genes,
831 but activates only a defined subset. Nucleic Acids Res. 2012;40:1509–22.

832 32. Lam KC, Mühlpfordt F, Vaquerizas JM, Raja SJ, Holz H, Luscombe NM,
833 et al. The NSL complex regulates housekeeping genes in Drosophila. PLoS
834 Genet. 2012;8:e1002736.

835 33. Mendjan S, Taipale M, Kind J, Holz H, Gebhardt P, Schelder M, et al.
836 Nuclear Pore Components Are Involved in the Transcriptional Regulation of
837 Dosage Compensation in Drosophila. Mol. Cell. 2006;21:811–23.

838 34. Lv W-W, Wei H-M, Wang D-L, Ni J-Q, Sun F-L. Depletion of histone
839 deacetylase 3 antagonizes PI3K-mediated overgrowth of Drosophila organs
840 through the acetylation of histone H4 at lysine 16. J. Cell Sci. 2012;125:5369–
841 78.

842 35. Smith ER, Pannuti A, Gu W, Steurnagel A, Cook RG, Allis CD, et al. The
843 drosophila MSL complex acetylates histone H4 at lysine 16, a chromatin
844 modification linked to dosage compensation. Mol. Cell. Biol. 2000;20:312–8.

845 36. van Berkum NL, Lieberman-Aiden E, Williams L, Imakaev M, Gnirke A,
846 Mirny LA, et al. Hi-C: A Method to Study the Three-dimensional Architecture
847 of Genomes. J. Vis. Exp. JoVE [Internet]. 2010 [cited 2016 Jul 6]; Available
848 from: http://www.ncbi.nlm.nih.gov/pmc/articles/PMC3149993/

849 37. Vogelmann J, Gall AL, Dejardin S, Allemand F, Gamot A, Labesse G, et
850 al. Chromatin Insulator Factors Involved in Long-Range DNA Interactions and
851 Their Role in the Folding of the Drosophila Genome. PLOS Genet.
852 2014;10:e1004544.

853 38. Eggert H, Gortchakov A, Saumweber H. Identification of the Drosophila
854 interband-specific protein Z4 as a DNA-binding zinc-finger protein determining
855 chromosomal structure. J. Cell Sci. 2004;117:4253–64.

856 39. Gan M, Moebus S, Eggert H, Saumweber H. The Chriz-Z4 complex
857 recruits JIL-1 to polytene chromosomes, a requirement for interband-specific
858 phosphorylation of H3S10. J. Biosci. 2011;36:425–38.

859 40. Hawkins RD, Hon GC, Lee LK, Ngo Q, Lister R, Pelizzola M, et al. Distinct
860 epigenomic landscapes of pluripotent and lineage-committed human cells.
861 Cell Stem Cell. 2010;6:479–91.

862 41. Shogren-Knaak M, Ishii H, Sun J-M, Pazin MJ, Davie JR, Peterson CL.
863 Histone H4-K16 acetylation controls chromatin structure and protein
864 interactions. Science. 2006;311:844–7.

865 42. Carrozza MJ, Li B, Florens L, Suganuma T, Swanson SK, Lee KK, et al.
866 Histone H3 methylation by Set2 directs deacetylation of coding regions by
867 Rpd3S to suppress spurious intragenic transcription. Cell. 2005;123:581–92.

868 43. Joshi AA, Struhl K. Eaf3 chromodomain interaction with methylated H3-
869 K36 links histone deacetylation to Pol II elongation. Mol. Cell. 2005;20:971–8.

870 44. Keogh M-C, Kurdistani SK, Morris SA, Ahn SH, Podolny V, Collins SR, et
871 al. Cotranscriptional set2 methylation of histone H3 lysine 36 recruits a
872 repressive Rpd3 complex. Cell. 2005;123:593–605.

873 45. Deng H, Zhang W, Bao X, Martin JN, Girton J, Johansen J, et al. The JIL-
874 1 kinase regulates the structure of Drosophila polytene chromosomes.
875 Chromosoma. 2005;114:173–82.

876 46. Gortchakov AA, Eggert H, Gan M, Mattow J, Zhimulev IF, Saumweber H.
877 Chriz, a chromodomain protein specific for the interbands of Drosophila
878 melanogaster polytene chromosomes. Chromosoma. 2005;114:54–66.

879 47. Rath U, Ding Y, Deng H, Qi H, Bao X, Zhang W, et al. The chromodomain
880 protein, Chromator, interacts with JIL-1 kinase and regulates the structure of
881 Drosophila polytene chromosomes. J. Cell Sci. 2006;119:2332–41.

882 48. Stampfel G, Kazmar T, Frank O, Wienerroither S, Reiter F, Stark A.
883 Transcriptional regulators form diverse groups with context-dependent
884 regulatory functions. Nature. 2015;528:147–51.

885 49. Bowman SK, Deaton AM, Domingues H, Wang PI, Sadreyev RI, Kingston
886 RE, et al. H3K27 modifications define segmental regulatory domains in the
887 Drosophila bithorax complex. eLife. 2014;3:e02833.

888 50. Holohan EE, Kwong C, Adryan B, Bartkuhn M, Herold M, Renkawitz R, et
889 al. CTCF genomic binding sites in Drosophila and the organisation of the
890 bithorax complex. PLoS Genet. 2007;3:e112.

891 51. Lowe N, Rees JS, Roote J, Ryder E, Armean IM, Johnson G, et al.
892 Analysis of the expression patterns, subcellular localisations and interaction
893 partners of Drosophila proteins using a pigP protein trap library. Dev. Camb.
894 Engl. 2014;141:3994–4005.

895 52. Dahl JA, Collas P. A rapid micro chromatin immunoprecipitation assay
896 (microChIP). Nat Protoc. 2008;3:1032–45.

897 53. Dahl JA, Collas P. MicroChIP--a rapid micro chromatin
898 immunoprecipitation assay for small cell samples and biopsies. Nucleic Acids
899 Res. 2008;36:e15.

900 54. Nicol JW, Helt GA, Blanchard SG, Raja A, Loraine AE. The Integrated
901 Genome Browser: free software for distribution and exploration of genome-
902 scale datasets. Bioinforma. Oxf. Engl. 2009;25:2730–1.

903 55. Hagège H, Klous P, Braem C, Splinter E, Dekker J, Cathala G, et al.
904 Quantitative analysis of chromosome conformation capture assays (3C-
905 qPCR). Nat. Protoc. 2007;2:1722–33.

906 56. Wingett S, Ewels P, Furlan-Magaril M, Nagano T, Schoenfelder S, Fraser
907 P, et al. HiCUP: pipeline for mapping and processing Hi-C data.
908 F1000Research. 2015;4:1310.

909 57. Mifsud B, Sugar R. GOTHiC: Binomial test for Hi-C data analysis. 2013;R
910 package version 1.6.0.

911 58. Lévy-Leduc C, Delattre M, Mary-Huard T, Robin S. Two-dimensional
912 segmentation for analyzing Hi-C data. Bioinformatics. 2014;30:i386–92.

913 59. Chintapalli VR, Wang J, Dow JAT. Using FlyAtlas to identify better
914 Drosophila melanogaster models of human disease. Nat. Genet.
915 2007;39:715–20.

916 60. Chen X, Lu C, Prado JR, Eun SH, Fuller MT. Sequential changes at
917 differentiation gene promoters as they become active in a stem cell lineage.
918 Development. 2011;138:2441–50.

919 61. Kwong C, Adryan B, Bell I, Meadows L, Russell S, Manak JR, et al.
920 Stability and dynamics of polycomb target sites in Drosophila development.
921 PLoS Genet. 2008;4:e1000178.

922 62. Taramasco O, Bauer S. RHmm: Hidden Markov Models simulations and
923 estimations. 2013;R package version 2.0.3.

924 63. ModENCODE. http://www.modencode.org.

925 64. Toedling J, Sklyar O, Huber W. Ringo – an R/Bioconductor package for
926 analyzing ChIP-chip readouts. BMC Bioinformatics. 2007;8:221.

927 65. Li L, Lyu X, Hou C, Takenaka N, Nguyen HQ, Ong CT, et al. Widespread
928 rearrangement of 3D chromatin organization underlies polycomb-mediated
929 stress-induced silencing. Mol Cell. 2015;58:216–31.

930 66. Wood AM, Van Bortle K, Ramos E, Takenaka N, Rohrbaugh M, Jones
931 BC, et al. Regulation of chromatin organization and inducible gene expression
932 by a Drosophila insulator. Mol. Cell. 2011;44:29–38.

933 67. Zhang Y, Liu T, Meyer CA, Eeckhoute J, Johnson DS, Bernstein BE, et al.
934 Model-based analysis of ChIP-Seq (MACS). Genome Biol. 2008;9:R137.

935 68. Cherbas L, Willingham A, Zhang D, Yang L, Zou Y, Eads BD, et al. The
936 transcriptional diversity of 25 Drosophila cell lines. Genome Res.
937 2011;21:301–14.

938 69. Sidiropoulos N, Sohi SH, Rapin N, Bagger FO. SinaPlot: an enhanced
939 chart for simple and truthful representation of single observations over
940 multiple classes [Internet]. 2015 Oct. Report No.: biorxiv;028191v1. Available
941 from: http://biorxiv.org/lookup/doi/10.1101/028191

942

943 **Figure Legends**

944 **Fig. 1 Domains with very low H3K27me3**

945 (a) Binding profiles of H3K27me3 in primary spermatocytes compared to Kc

946 cell and 0-12 hr embryo H3K27me3 profiles and Kc cell Polycomb profile.

947 Green bars indicate selected regions of very low H3K27me3 and red bars
948 indicate selected Polycomb binding regions. See Table S2 for data sources.
949 (b) SinaPlots [69] of H3K27me3 median binding scores at the TSSs (+/-
950 500bp) of different gene classes: all = all genes in euchromatic genome, hk =
951 housekeeping genes, Sp = spermatogenesis genes, nT = genes not
952 expressed in testis, Pc = Polycomb targets from [61], see Methods for
953 derivation of gene classes. Means are indicated by horizontal lines. (c) Scatter
954 plot of H3K27me3 median binding scores at all TSSs (+/- 500bp) for pupae
955 versus primary spermatocytes showing distinct clustering of the different gene
956 classes. (d) Relative distance of the mean of the spermatogenesis gene class
957 binding scores at TSSs, in reference to the hk mean as zero and the Pc mean
958 as 1, at different developmental stages (E = Embryo, L1-3 = Larval instars, F
959 = adult female and M = adult male), in cell lines (Kc and S2) and in primary
960 spermatocytes (Sp). There is a trend of increasing H3K27me3 during
961 development.
962
963 **Fig. 2 Genomic features of D domains**
964 (a) Profiles of selected histone modifications, chromatin components and
965 housekeeping genes show association with the D domain HMM state (green
966 bars) based on the H3K27me3 profile in primary spermatocytes. The
967 H3K27me3 and H3K27me2 profiles both show low levels in the D domains
968 but differ in the Pc target regions (red bars). (b) Stacked plots of scaled D
969 domains (left) and E domains (right) showing enrichment of tiles containing
970 housekeeping gene TSSs in D domains. D and E regions are split into 80
971 equal sized tiles per region and extended on both sides by 10 tiles outside the

region. Red dotted lines show domain borders. (c) Using the 5-state colour-coded chromatin state classification of Filion et al. [1], the plot shows the different chromatin state proportions in D and E domains and the prevalence of the "yellow" state in D domains. (d) Using cell line gene expression data from Cherbas et al. [68], the plot shows that genes with narrow tissue expression are more prevalent in E domains (blue), whereas genes with broad expression are more prevalent in D domains (green). (e) Boxplots of ChIP scores for histone modifications across D (green) and E (blue) domains showing depletion of repressive chromatin modifications and enrichment of active chromatin modification in D domains. (f) Boxplots of ChIP scores for selected chromatin components showing enrichment in D domains. See Table S2 for data sources.

Fig. 3 D domains are strongly associated with TAD architecture

(a) Heatmap of 10kb binned normalised HiC interactions across a 2 Mb region of chromosome 2L in Kc cells showing the association of the D domain state and TAD architecture. Below the interaction heatmap the tracks are "H3K27me3" showing the H3K27me3 primary spermatocyte profile, "D" showing the D HMM-defined domains, "HiC" showing the TAD boundaries derived from the Kc cell HiC data and "State" showing the 5-colour chromatin state profile. (b) Histograms showing (from the left) the mapping of D domain borders to Kc HiC TAD boundaries (D to Kc TAD) and vice versa (Kc TAD to D), followed by the mapping of the D domains borders to the TAD boundaries identified in embryo chromatin by Sexton et al. [9] (D to Embryo TAD) and vice versa (Embryo TAD to D). (c) In contrast to model "*a*" where TADs abut

997 at simple interfaces, we suggest model "*b*" where prominent TADs (blue) are
998 separated by boundary regions corresponding to D domains (green).
999
1000 **Fig. 4 D domains and Insulators**
1001 (a) Binding profiles of insulator and insulator-related components showing that
1002 a subset, Chromator, BEAF-32, Z4/Putzig and JIL-1, show a clear association
1003 with D domains (green bars) whereas CTCF does not. All profiles are from Kc
1004 cells, see Table S2 for data sources. (b) Percentages of TSSs, DNase1 sites,
1005 insulator and insulator-related components mapping to D or E domains. (c)
1006 Profiles of insulator/insulator-related components within a single D domain.
1007 The binding sites of these components are spread throughout the domain and
1008 show an association with TSSs and not with the domain boundaries. The
1009 extent of the D domain is represented by the green bar, TSSs are indicated by
1010 grey bars and genes in the housekeeping gene list are indicated by gold
1011 asterisks. (d) Plots showing mapping of insulator/insulator-related
1012 components to scaled D (green line) and E (blue line) domains. D and E
1013 domains are split into 80 tiles per domain and extended on both sides by 10
1014 tiles. The number of normalized binding summits were counted for each tile.
1015 For normalisation, the summit counts were scaled by the number of summit
1016 binding positions (n) for each factor so that each summit count is 1000/n. The
1017 dotted vertical lines indicate the domain borders. For the TSS plot, "counts" is
1018 the number of TSSs per tile. The binding locations are evenly spread
1019 throughout D domains and not concentrated at the domain borders. For E
1020 domains, the flanking peaks are likely due to the scaling causing compression
1021 of large domains and a similar profile is seen with insulator/insulator-related

and TSS mapping. (e) Accumulation plots focused on either TSSs or domain borders. In the TSS plots the red line indicates housekeeping genes and the grey line indicates non-housekeeping genes. The total summit counts for each factor are scaled as in (d), normalised to correct for the different numbers of TSSs and Borders and the final values scaled to give a range between 0-10.

Fig. 5 D and E domains are topologically distinct

(a) Kc Hi-C interaction heatmaps at selected D and E domains with tracks “D” showing the D domain as green bars, “HiC” showing the derived TAD boundaries and “State” showing the 5-colour chromatin state profile. Whilst the E region TADs show rather uniform interaction across the whole domain, in the D regions there is a prevalence of short interactions with high heatmap intensity close to the baseline. (b) Interaction distance profile for D domains (green line) and E domains (blue line) showing the preponderance of short interactions in D domains. For both D and E regions longer than 30kb (D = 443 regions, E = 755 regions) the normalised HiC interaction counts (10kb resolution) were collected into 10kb distance bins and the median per bin calculated. The p-value was calculated using the Wilcox test of the medians between D and E. (c) Profiles of interaction distance across a 5 Mb region on Chromosome X (see Methods for details). D domains are indicated by green bars. The “far” interaction (50-500kb) frequency dips in D domains (top profile), whilst the “close” interaction (5-50kb) frequency peaks in D domains. The bottom profile shows the ratio of “close”/“far” interactions.

Fig. 6 Inter-domain interactions

(a) Kc Hi-C interaction heatmaps at selected D and E domains showing evidence of interaction between D domains. The “D” track shows D domains (green bars). (b) Schematic of interaction heatmap showing inter-domain interactions. (c) Model of chromatin organization into D (green) and E (blue) domains. The two domains types are represented with different chromatin topologies with the E domains condensed and the D domains more open but with defined short-range interactions mediated by insulator complexes (yellow discs). D and E domains are represented as spatially segregated fitting the observation of interaction between domains of the same type.

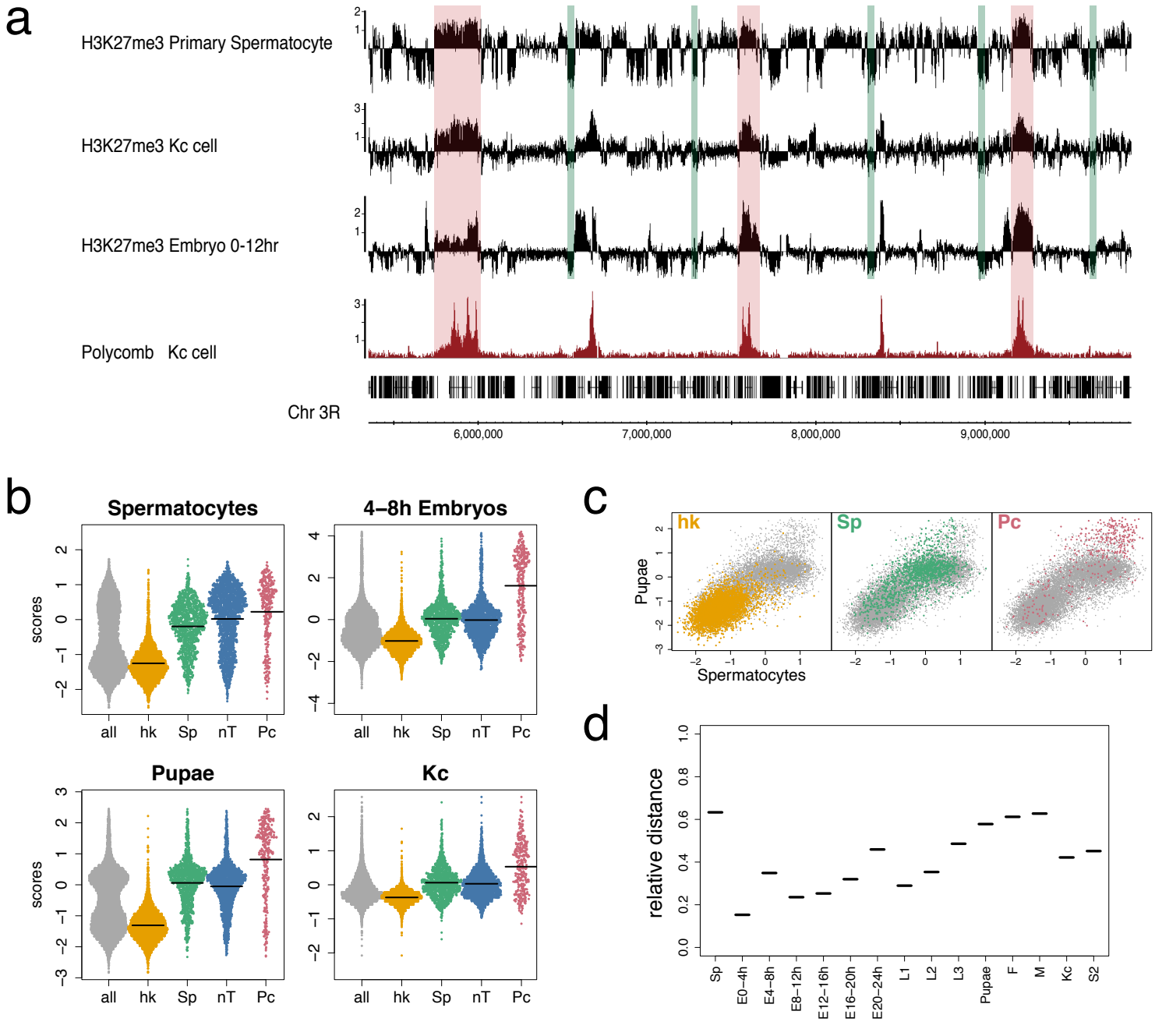
a
H3K27me3 Primary Spermatocyte
H3K27me3 Kc cell
H3K27me3 Embryo 0-12hr
Polycomb Kc cell
Chr 3R
6,000,000
7,000,000
8,000,000
9,000,000
b
Spermatocytes
4–8h Embryos
Pupae
Kc
scores
all
hk
Sp
nT
Pc
c
hk
Sp
Pc
Pupae
Spermatocytes
d
relative distance
Sp
E0–4h
E4–8h
E8–12h
E12–16h
E16–20h
E20–24h
L1
L2
L3
Pupae
F
M
Kc
S2

Figure 1

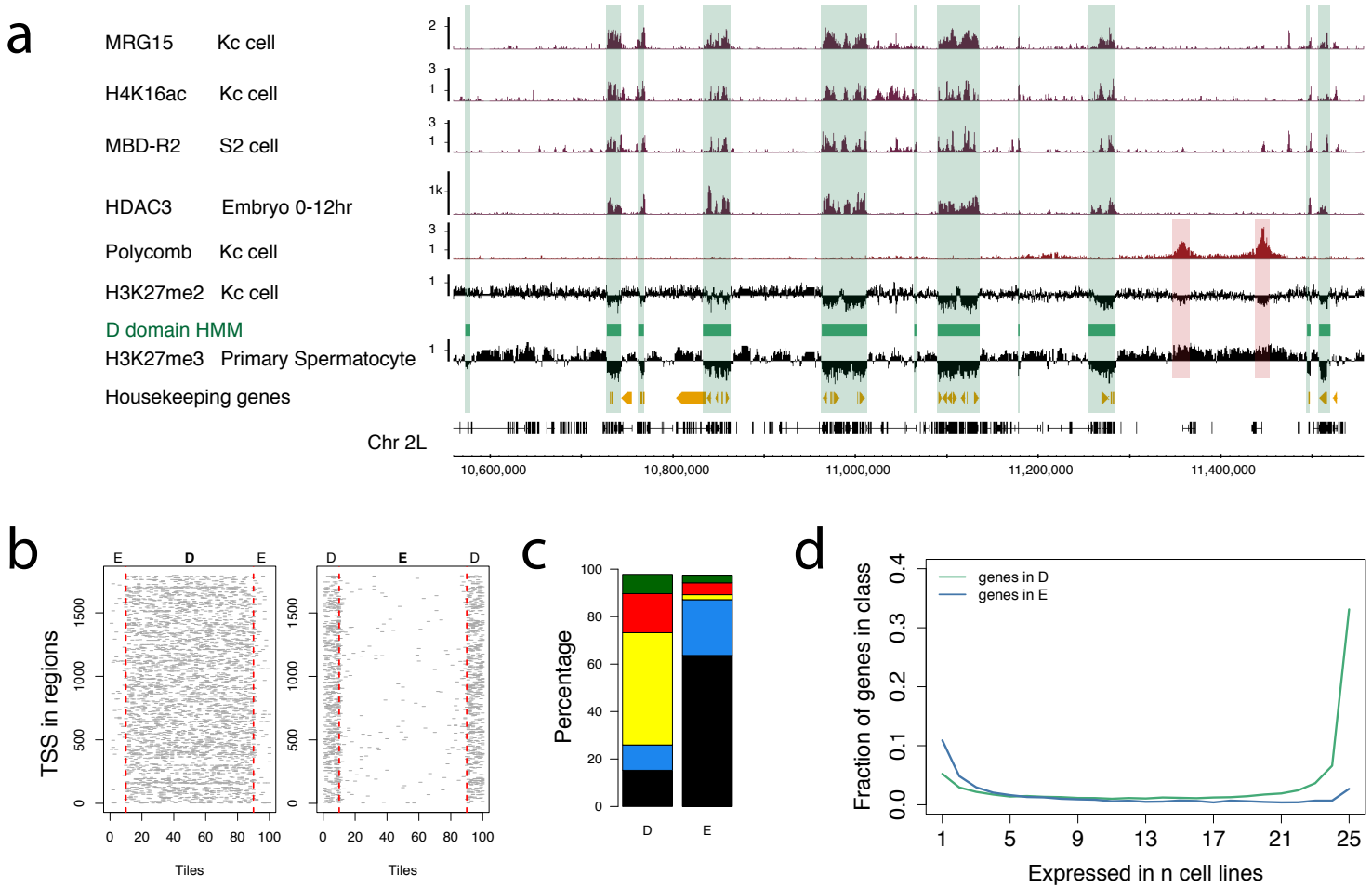
a
MRG15 Kc cell
H4K16ac Kc cell
MBD-R2 S2 cell
HDAC3 Embryo 0-12hr
Polycomb Kc cell
H3K27me2 Kc cell
D domain HMM
H3K27me3 Primary Spermatocyte
Housekeeping genes
Chr 2L
10,600,000
10,800,000
11,000,000
11,200,000
11,400,000
b
TSS in regions
Tiles
Tiles
c
Percentage
D
E
d
genes in D
genes in E
Fraction of genes in class
Expressed in n cell lines
e
H3K27me2
H3K27me3
H3K27ac
H3K36me3
H3K4me3
H3K9ac
H4K16ac
median scores
f
HDAC1
HDAC3
MBD−R2
MRG15
median scores

Figure 2

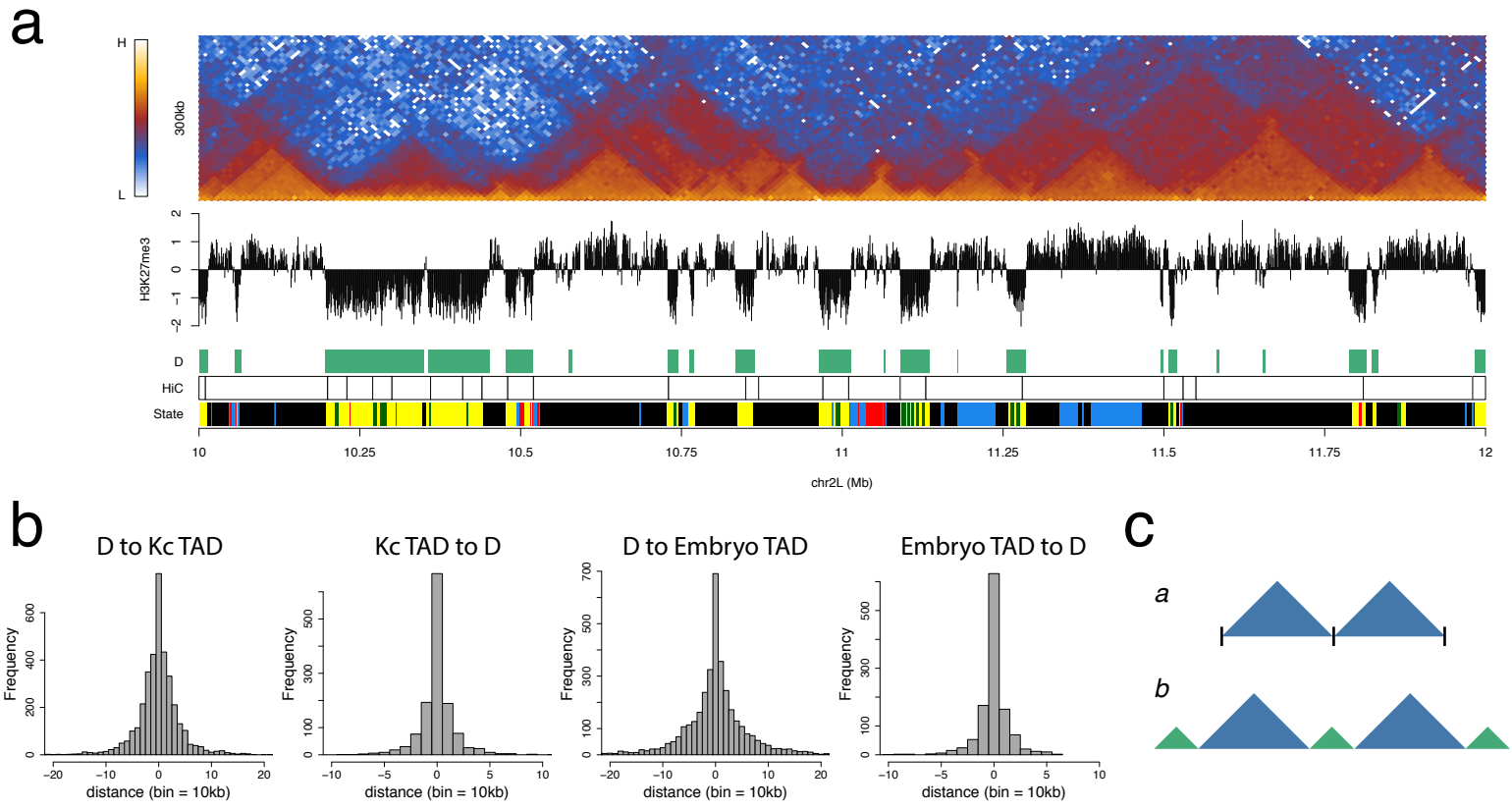
a
H
L
300kb
H3K27me3
D
HiC
State
10
10.25
10.5
10.75
11
11.25
11.5
11.75
12
chr2L (Mb)
b
D to Kc TAD
Kc TAD to D
D to Embryo TAD
Embryo TAD to D
Frequency
distance (bin = 10kb)
c
a
b

Figure 3

a

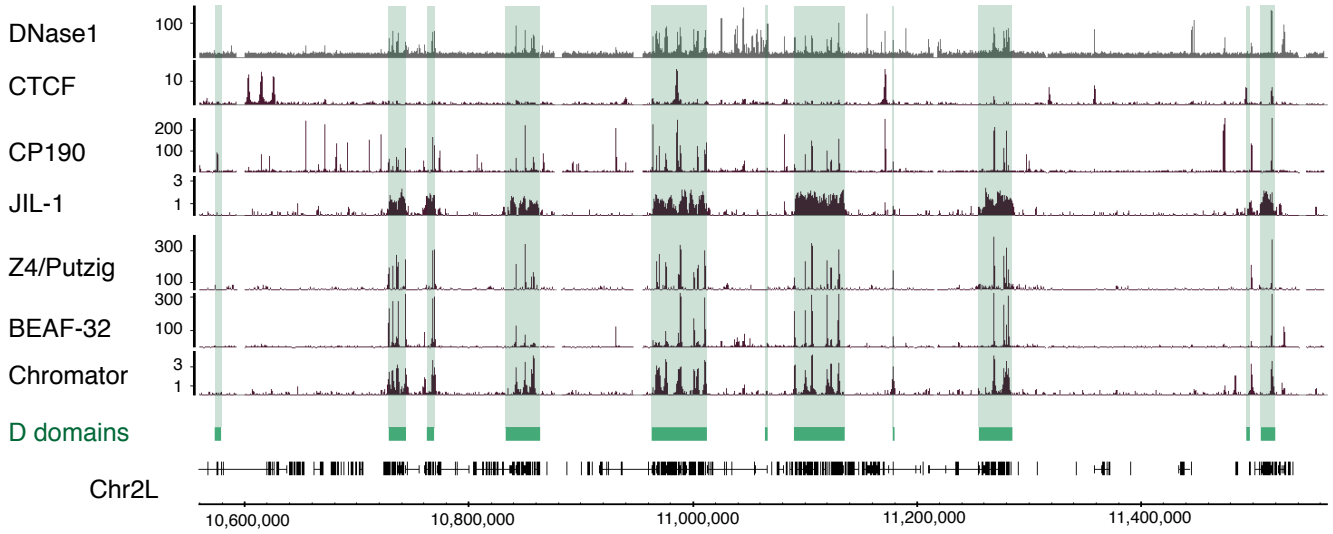

b

	% D	% E
TSS	61.6	38.4
Z4/Putzig	95.8	4.2
Jil1	88.1	11.9
Chromator	87.6	12.4
BEAF	85.9	14.1
DNAse1	76.0	24.0
CP190	66.5	33.5
GAF	66.5	33.5
CTCF	57.0	43.0
Su(Hw)	25.5	74.5

c

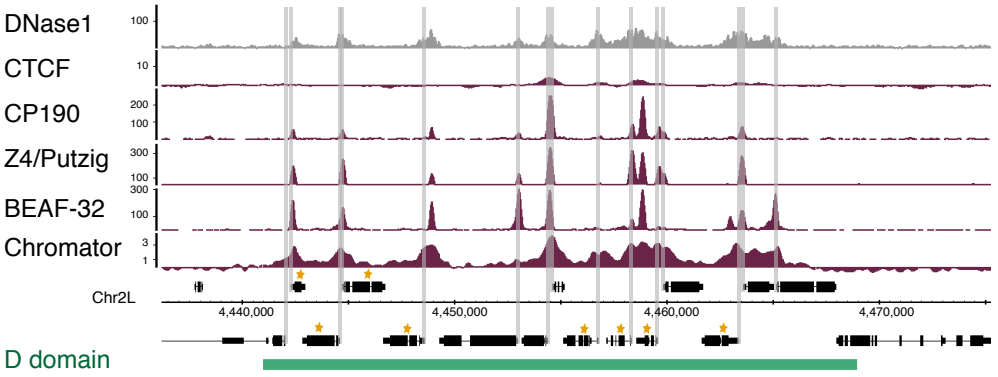

d

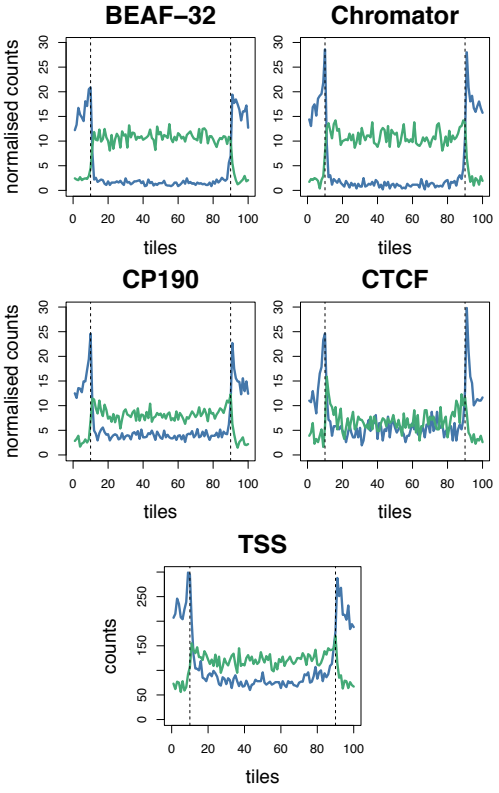

e

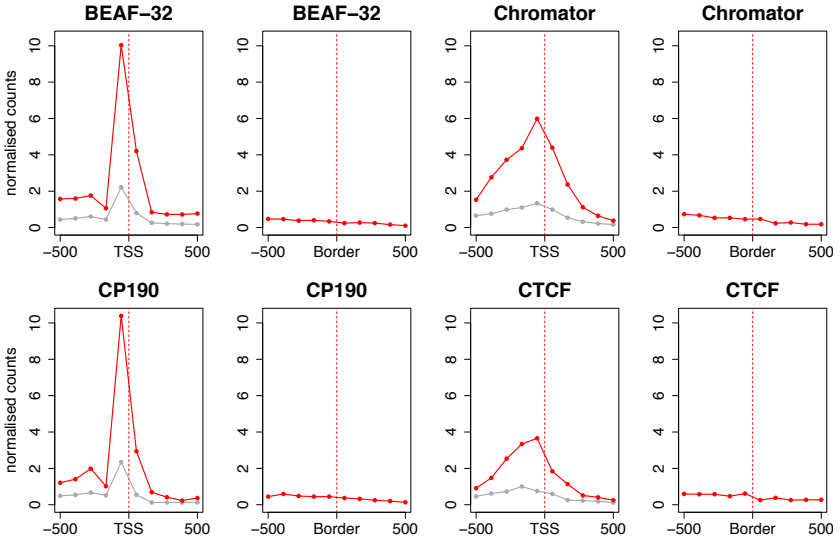

Figure 4

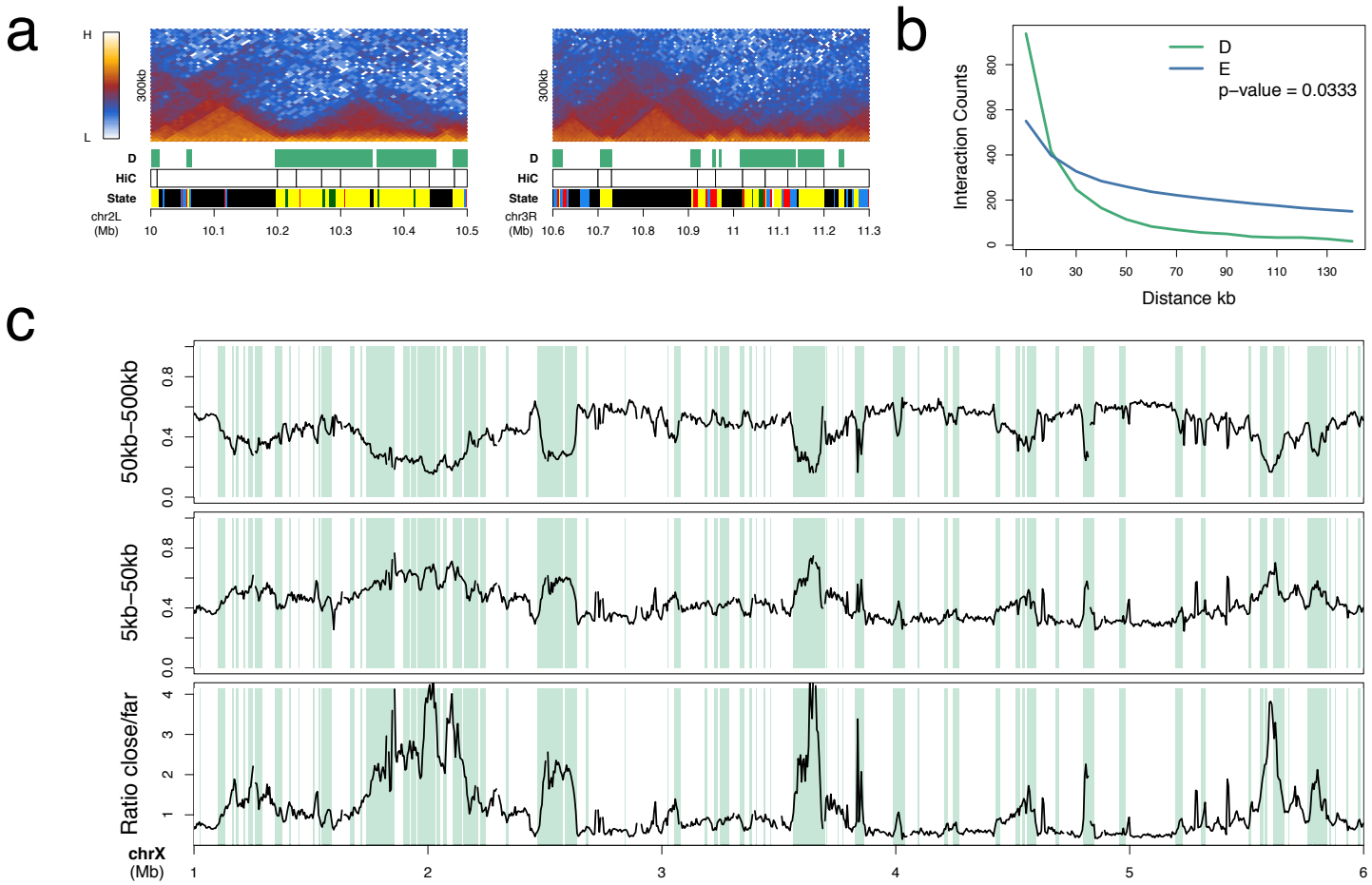
a
H
L
300kb
D
HiC
State
chr2L
(Mb)
10
10.1
10.2
10.3
10.4
10.5
chr3R
10.6
10.7
10.8
10.9
11
11.1
11.2
11.3
b
Interaction Counts
D
E
p−value = 0.0333
Distance kb
c
50kb−500kb
5kb−50kb
Ratio close/far
chrX
(Mb)

Figure 5

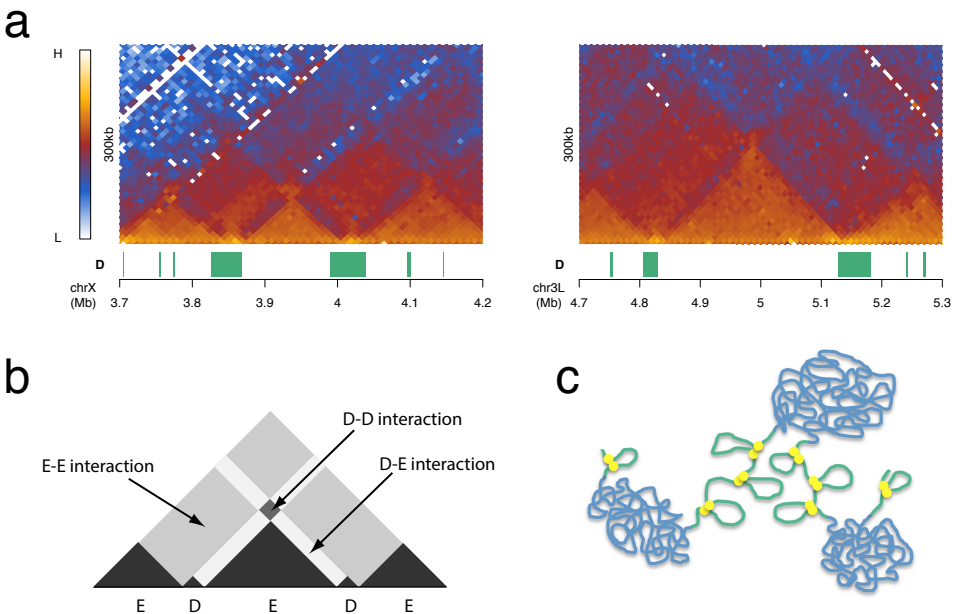
a
H
L
300kb
D
chrX
(Mb)
3.7
3.8
3.9
4
4.1
4.2
300kb
D
chr3L
(Mb)
4.7
4.8
4.9
5
5.1
5.2
5.3
b
D-D interaction
E-E interaction
D-E interaction
E
D
E
D
E
c

Figure 6